Interplay between Side Chain Density and Polymer Alignment: Two Competing Strategies for Enhancing the Thermoelectric Performance of P3HT Analogues

Peter Gilhooly-Finn, Ian Jacobs, Olivier Bardagot, Yasser Zaffar, Antoine Lemaire, Shubhradip Guchait, Lu Zhang, Mark Freeley, William Neal, Fanny Richard, et al.

▶ **To cite this version:**

Peter Gilhooly-Finn, Ian Jacobs, Olivier Bardagot, Yasser Zaffar, Antoine Lemaire, et al.. Interplay between Side Chain Density and Polymer Alignment: Two Competing Strategies for Enhancing the Thermoelectric Performance of P3HT Analogues. Chemistry of Materials, 2023, 10.1021/acs.chemmater.3c01680 . hal-04265399

HAL Id: hal-04265399
https://hal.science/hal-04265399

Submitted on 30 Oct 2023

HAL is a multi-disciplinary open access archive for the deposit and dissemination of scientific research documents, whether they are published or not. The documents may come from teaching and research institutions in France or abroad, or from public or private research centers.

L'archive ouverte pluridisciplinaire **HAL**, est destinée au dépôt et à la diffusion de documents scientifiques de niveau recherche, publiés ou non, émanant des établissements d'enseignement et de recherche français ou étrangers, des laboratoires publics ou privés.

This document is confidential and is proprietary to the American Chemical Society and its authors. Do not copy or disclose without written permission. If you have received this item in error, notify the sender and delete all copies.

The Interplay Between Side Chain Density and Polymer Alignment: Two Competing Strategies for Enhancing the Thermoelectric Performance of P3HT Analogues

Journal:	*Chemistry of Materials*
Manuscript ID	cm-2023-01680j.R3
Manuscript Type:	Article
Date Submitted by the Author:	06-Oct-2023
Complete List of Authors:	Gilhooly-Finn, Peter; University College London, Department of Chemistry Jacobs, Ian; University of Cambridge, Cavendish Laboratory Bardagot, Olivier; University of Bern, Department of Chemistry Zaffar, Yasser; Queen Mary University of London, Department of Chemistry Lemaire, Antoine; CNRS, Institut Charles Sadron Guchait, Shubhradip; Institut Charles Sadron, Physics of Polymeric and Molecular Mat. Zhang, Lu; University of Cambridge, Cavendish Laboratory Freeley, Mark; Queen Mary University of London, Department of Chemistry Neal, William; Queen Mary University of London, Department of Chemistry Richard, Fanny; Universite de Strasbourg, ICPEES Palma, Matteo; Queen Mary University of London, Department of Chemistry & Biochemistry School of Physical and Chemical Sciences Banerji, Natalie; University of Bern, Department of Chemistry and Biochemistry; Sirringhaus, Henning; University of Cambridge, Cavendish Laboratory Brinkmann, Martin; Institut Charles Sadron, Physics of Polymeric and Molecular Mat. Nielsen, Christian; Queen Mary University of London, Materials Research Institute

SCHOLARONE™
Manuscripts

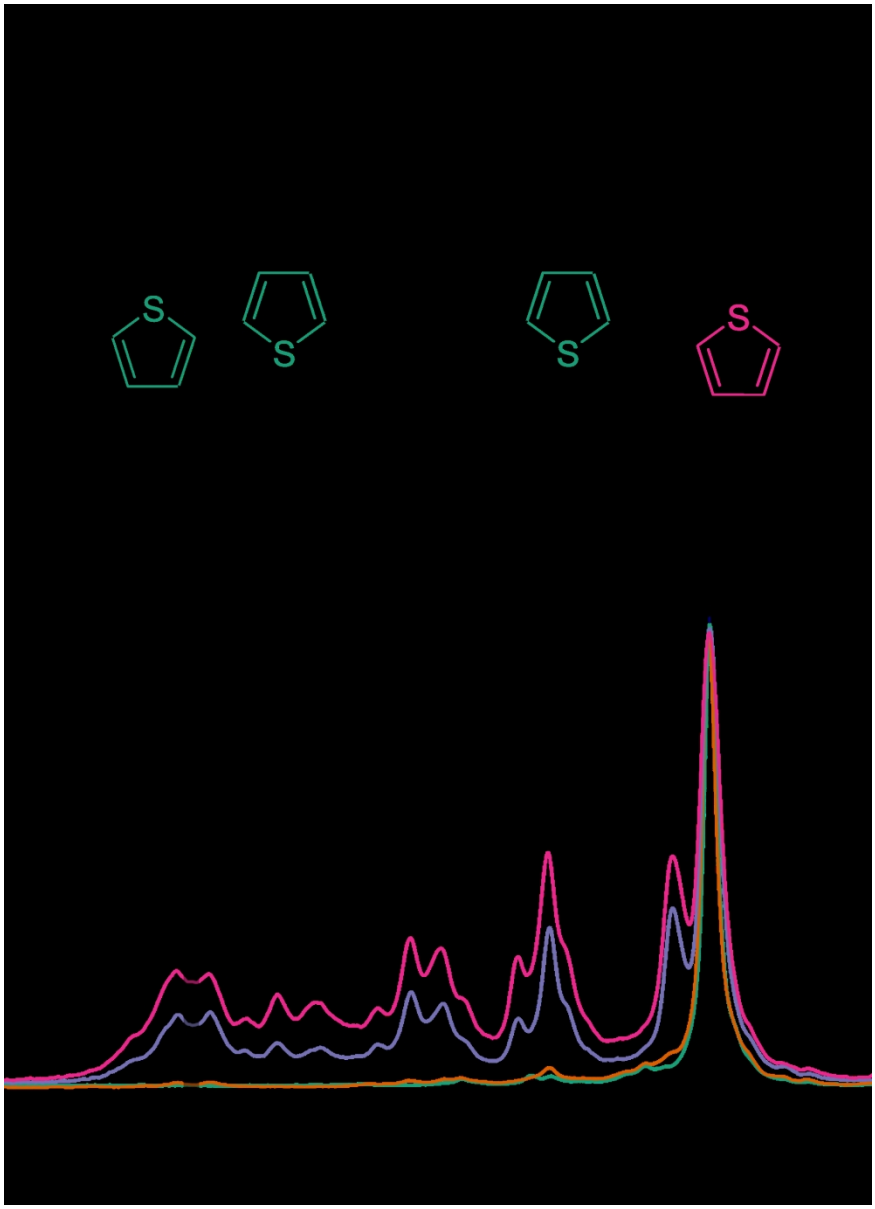

Figure 1. Representation of P3HT (left) and poly(3-hexylthiohene-ran-thiophene) (right). Green and pink thiophene units represent monomers with and without side chains respectively. x represents the mol% of unsubstituted thiophene. Superimposed 1H NMR spectra of P3HT (green), Tref (yellow), T19 (purple) and T24 (pink) focusing on the aromatic region (bottom).

155x214mm (330 x 330 DPI)

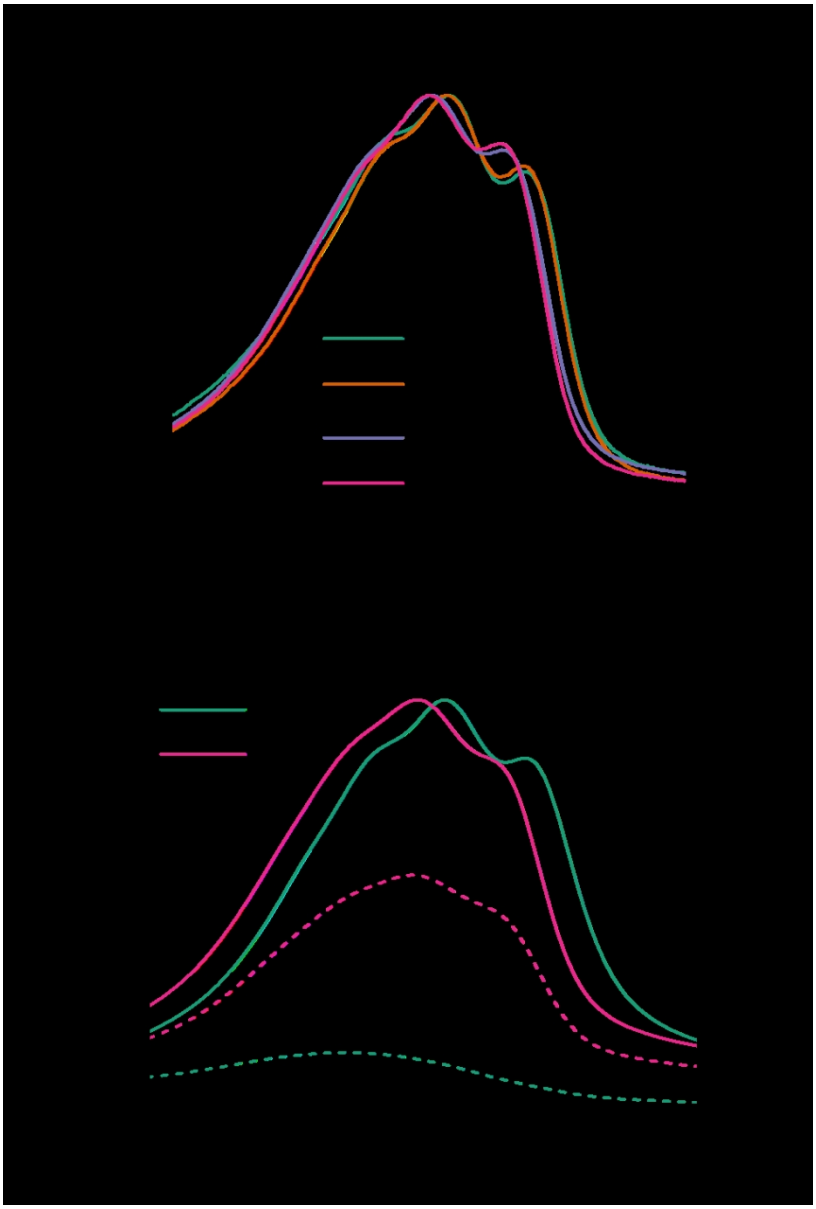

Figure 2. (top) UV-Vis absorbance spectra of P3HT, T_{ref}, T19 and T24 films spin-cast from 10 mg mL^{-1} o-dichlorobenzene (ODCB) solutions at 2000 rpm for 90 seconds. The spectra are normalised to the lambda max. (bottom) Polarised UV-Vis spectra of P3HT and T24 aligned films in the parallel (solid line) and perpendicular (dashed line) direction to the rubbing direction. P3HT and T24 films were rubbed at 220 °C and 80 °C respectively. The transitions in the parallel and perpendicular direction to the rubbing direction are normalised to the lambda max of the transition in the parallel direction.

75x111mm (330 x 330 DPI)

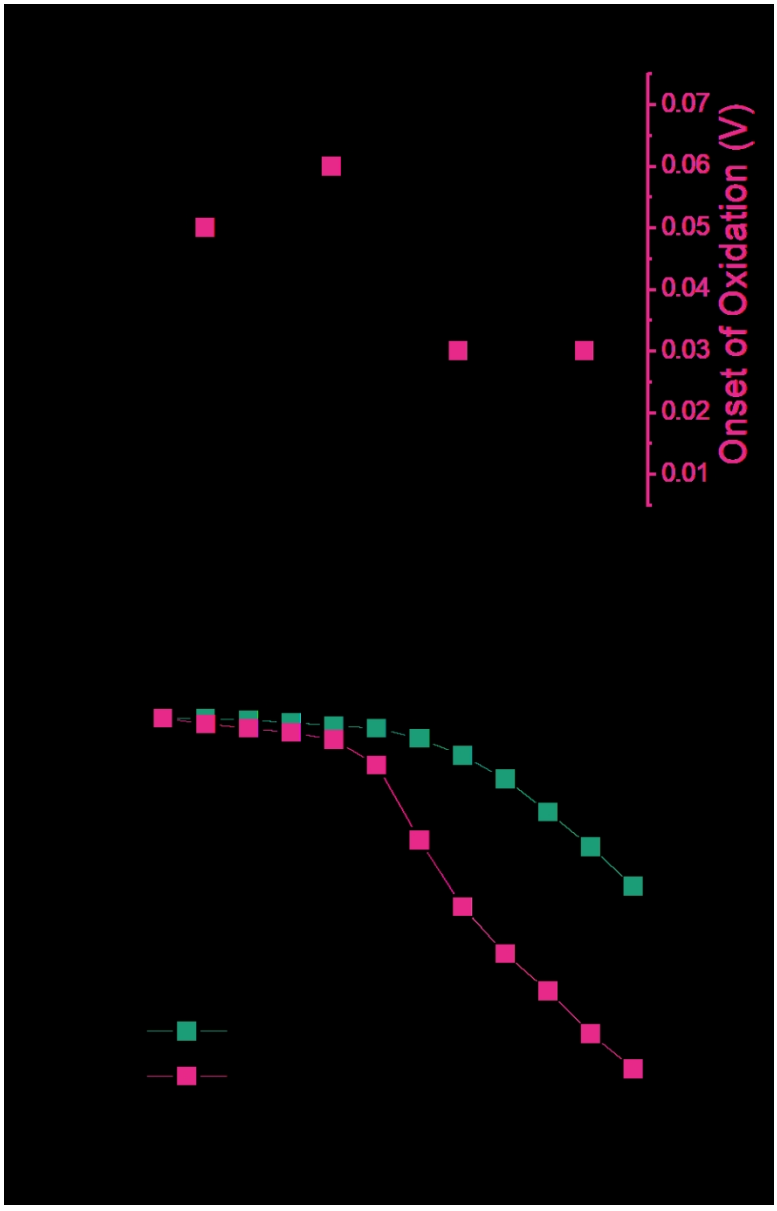

Figure 3. (top) Plot showing the correlations between work function and onset of electrochemical oxidation across the polymer series. The work function was obtained via the aver-age of two PESA measurements on 10 mg mL^{-1} ODCB solutions doctor-bladed onto ITO substrates and the onset of oxidation was taken from the onset of the minor oxidation peak from the CV measurements at a scan rate of 50 mV s^{-1}. (bottom) Plot of the decrease in absorption of the π-π* transition of P3HT and T24 thin films spin-cast from 10 mg mL^{-1} ODCB solutions onto ITO-coated glass with increasing electrochemical potential. Each spectrum was taken 1 minute after the applied potential. The trend is normalised to the λ_{max} of the first spectrum taken in the undoped state.

70x110mm (330 x 330 DPI)

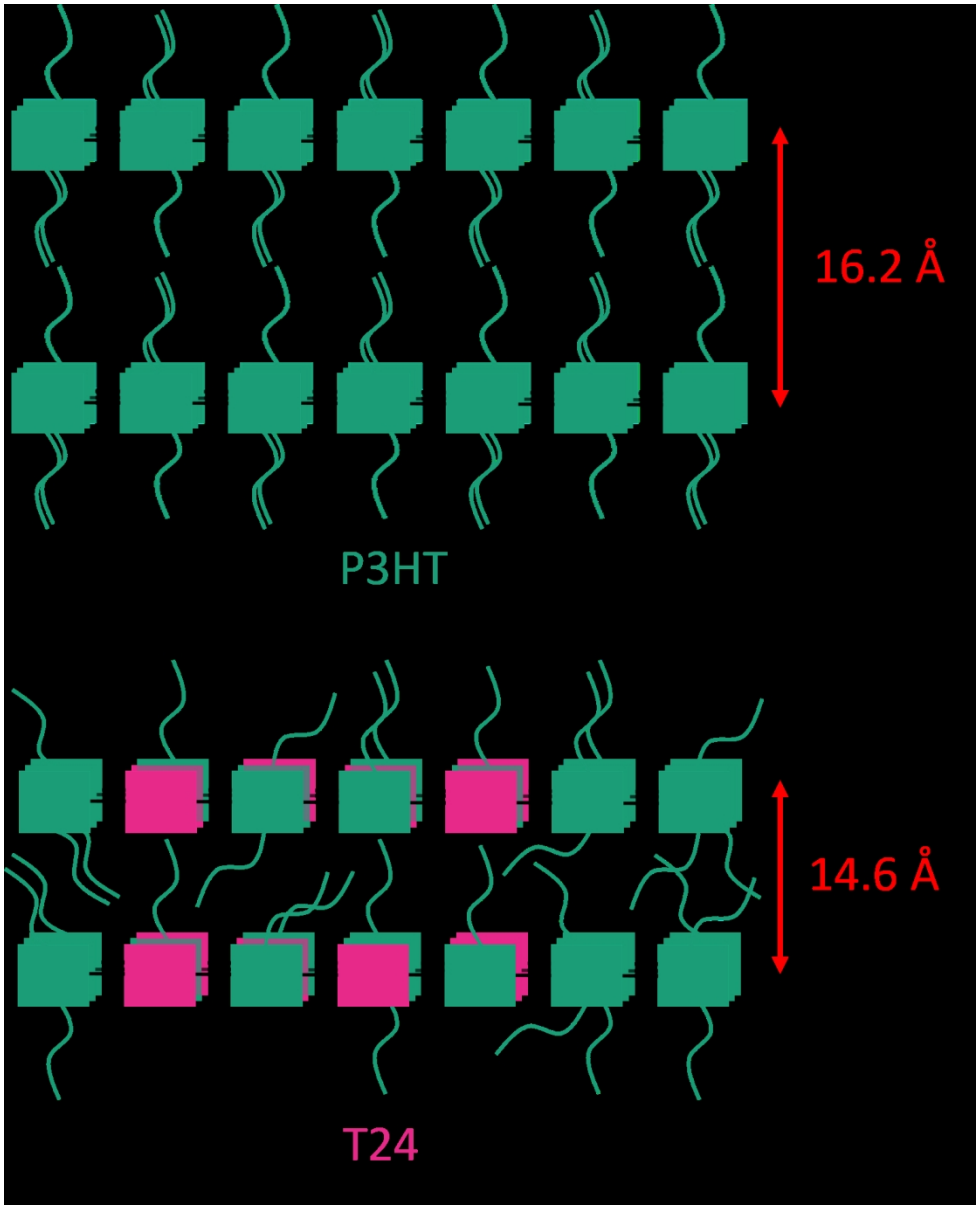

Figure 4. Schematic suggesting how the side chains fill empty space between the polymer backbones for T24 compared to P3HT, interpreted from the diffraction data of the non-aligned films. Green and pink squares represent thiophene monomers with and without a hexyl side chain respectively.

120x149mm (330 x 330 DPI)

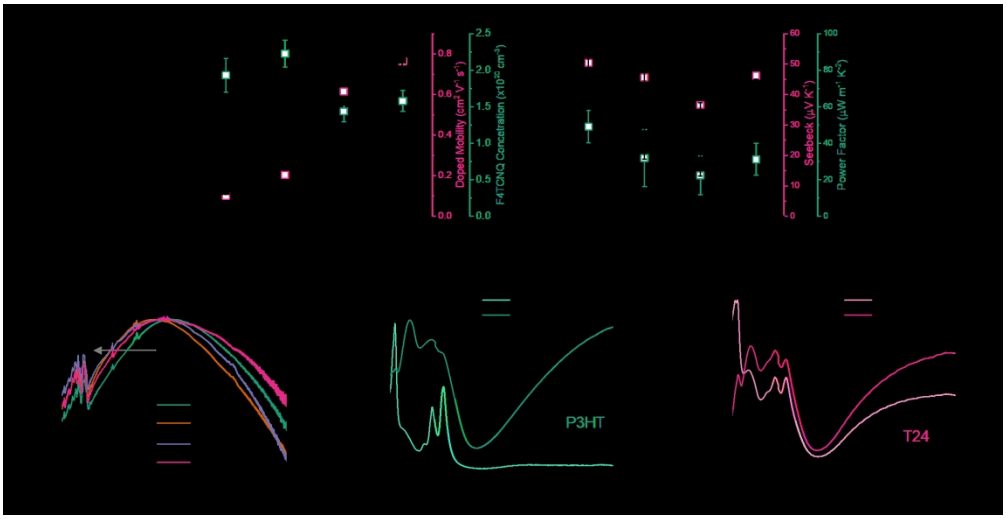

Figure 5. a) Plot showing the correlation between the measured electrical conductivity (black filled data points), estimated F4TCNQ radical anion concentration (pink filled) and estimated doped mobility (green open) for non-aligned P3HT and co-polymer thin films doped with F4TCNQ using HighSqP doping levels. The error bars arise from one standard deviation over 3 thickness measurements on one film and propagated through the Van der Pauw equation. b) Plot showing the correlation between the electrical conductivity (black filled), Seebeck Coefficient (pink open) and Power Factor (green open) in the parallel direction to the rubbing direction of aligned films doped with F4TCNQ at 1 mg mL^{-1}. The error bar in electrical conductivity arises from one standard deviation over two measurements of two devices. The error bar in power factor in propagated through $PF = \sigma S^2$ where σ and S are the electrical conductivity and Seebeck coefficient respectively. See supplementary information section 14 for thickness calculations. c) FTIR spectra of P3HT and co-polymer doped non-aligned films. The arrow indicates to the reader the shift in the peak at ~4000 cm^{-1}. d,e) UV-Vis-NIR spectra of P3HT (d) and T24 (e) aligned films doped with F4TCNQ using ICD up to 1 mg mL^{-1} measured in the perpendicular and parallel directions to the rubbing direction.

169x86mm (330 x 330 DPI)

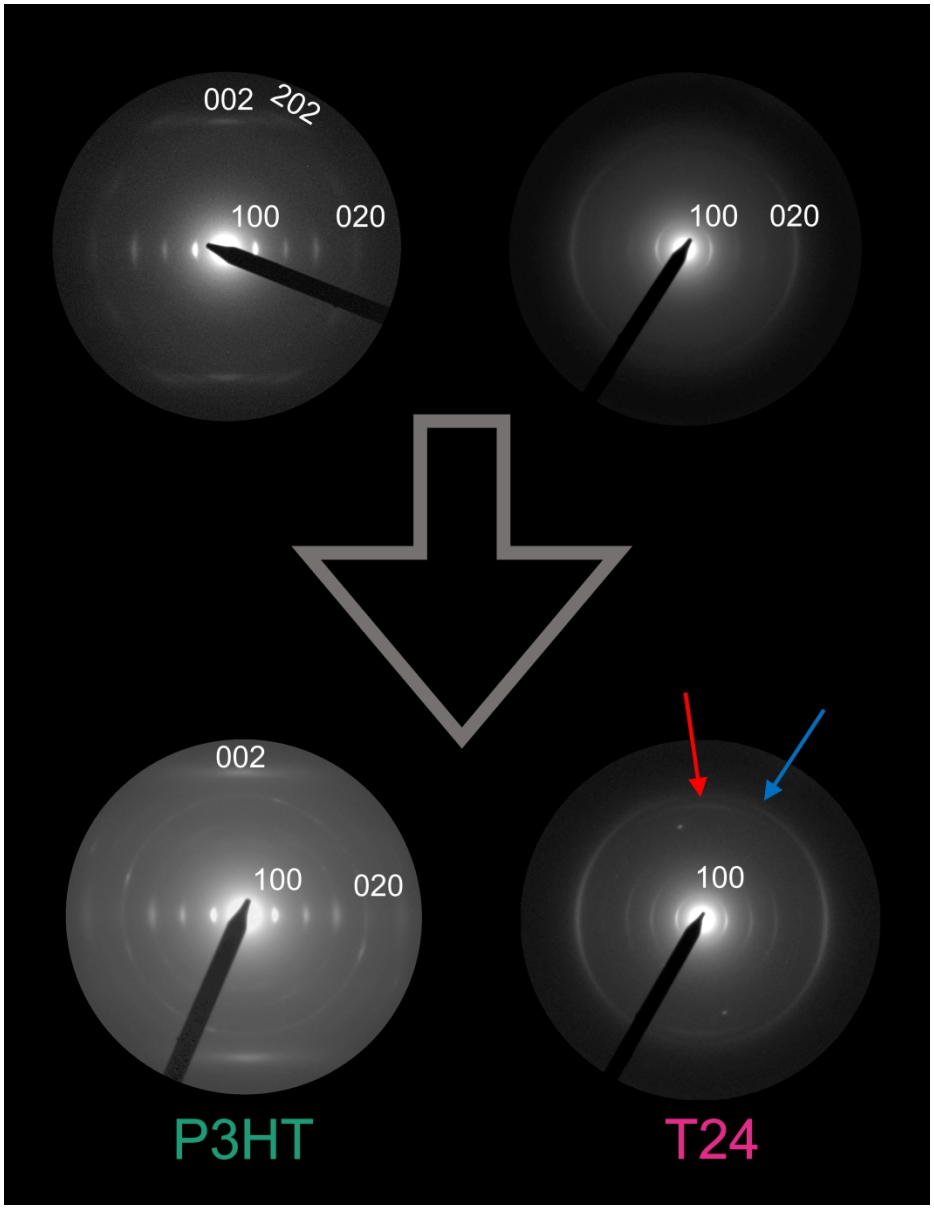

Figure 6. Electron diffraction patterns of P3HT and T24 aligned films before and after doping with F4TCNQ concentration of 1 mg mL^{-1}. The 'R' arrows represent the rubbing direction. The red and blue arrows direct the reader to the (002) and (020) reflection after doping to 1 mg mL^{-1} for T24 aligned films.

259x335mm (330 x 330 DPI)

The Interplay Between Side Chain Density and Polymer Alignment: Two Competing Strategies for Enhancing the Thermoelectric Performance of P3HT Analogues

Peter A. Gilhooly-Finn*[†,‡], Ian E. Jacobs[§], Olivier Bardagot[||], Yasser Zaffar[‡], Antoine Lemaire[#], Shubhradip Guchait[#], Lu Zhang[§], Mark Freeley[‡], William Neal[‡], Fanny Richard[††], Matteo Palma[‡], Natalie Banerji[||], Henning Sirringhaus[§], Martin Brinkmann[#] and Christian B. Nielsen*[‡]

[†]Department of Chemistry, University College London, Gower Street, London, WC1E 6BT, UK.

[‡]Department of Chemistry, Queen Mary University of London, Mile End Road, E1 4NS, London, UK.

[§]Optoelectronics Group, University of Cambridge, Cavendish Laboratory, J J Thomson Avenue, Cambridge, CB3 0HE, UK.

[||]Department of Chemistry, Biochemistry and Pharmaceutical Sciences, University of Bern, Freiestrasse 3, 3012 Bern, Switzerland.

[#]Charles Sadron Institute (ICS), CNRS Université de Strasbourg, UPR 22, 23 rue du Loess, Strasbourg Cedex 02, 67034, France.

[††]Université de Strasbourg, CNRS, ISIS UMR 7006, Strasbourg 67000, France.

ABSTRACT: A series of polythiophenes with varying side chain density was synthesised, and their electrical and thermoelectric properties were investigated. Aligned and non-aligned thin films of the polymers were characterised in the neutral and chemically doped states. Optical and diffraction measurements revealed an overall lower order in the thin films with lower side chain density, also confirmed using polarised optical experiments on aligned thin films. However, upon doping of the non-aligned films, a six-fold increase in electrical conductivity was observed for the polythiophene with lowest side chain density compared to poly(3-hexylthiophene) (P3HT). We found that the improvement in conductivity was not due to a larger charge carrier density, but an increase in charge carrier mobility after doping with 2,3,5,6-tetrafluoro-7,7,8,8-tetracyanoquinodimethane (F4TCNQ). On the other hand, doped aligned films did not show the same trend; lower side chain density instead led to a lower conductivity and Seebeck coefficient compared to P3HT. This was attributed to poorer alignment of the polymer thin films with lower side chain density. The study demonstrates that optimising side chain density is a synthetically simple and effective way to improve electrical conductivity in polythiophene films relevant for thermoelectric applications.

INTRODUCTION

Organic semiconducting polymers are emerging as viable candidates for thermoelectric devices, in particular for low-grade heat harvesting and for applications where conformability is important.[1, 2] Side chains for organic semiconductors are crucial for solubilising, otherwise insoluble, polymers allowing device fabrication by solution processing.[3] In addition to other advantages, side chains can also induce highly ordered solid-state morphologies needed for high charge transport.[4] However, for organic semiconductors to be realised as a potential thermoelectric material, high charge mobility needs to be coupled with high charge carrier density, to improve their intrinsically low electrical conductivity.[5]

Increasing the charge carrier density can be achieved via doping, either chemically (also known as molecularly) or electrochemically, utilising redox reactions that add an electron to the lowest unoccupied molecular orbital (LUMO) or remove an electron from the highest occupied molecular orbital (HOMO) for n-type and p-type doping, respectively. The chemical doping method is one of the most widely used techniques to improve the charge carrier density, and therefore the electrical conductivity, in an organic semiconducting polymer. For p-type doping, strong electron acceptors such as 2,3,5,6-tetrafluoro-7,7,8,8-tetracyanoquinodimethane (F4TCNQ), Mo(tfd-$COCF_3$)$_3$ and iron chloride ($FeCl_3$) are frequently used in conjunction with electron rich semiconducting polymers such as poly(3-hexylthiophene) (P3HT) and poly[2,5-bis(3-tetradecylthiophen-2-yl)thieno[3,2-b]thiophene] (PBTTT). On the other hand, n-type chemical doping is traditionally accomplished via a hydride source such as 4-(2,3-Dihydro-1,3-dimethyl-1H-benzimidazol-2-yl)-N,N-dimethylbenzenamine (N-DMBI) and its derivates.[6] Improvement in doping procedures have progressed from blending of the dopant and organic semiconductor to sequential doping techniques. Sequential doping

techniques enable the highly ordered solid state morphology to be retained to some extent due to the use of an orthogonal solvent. Utilising the sequential doping method,

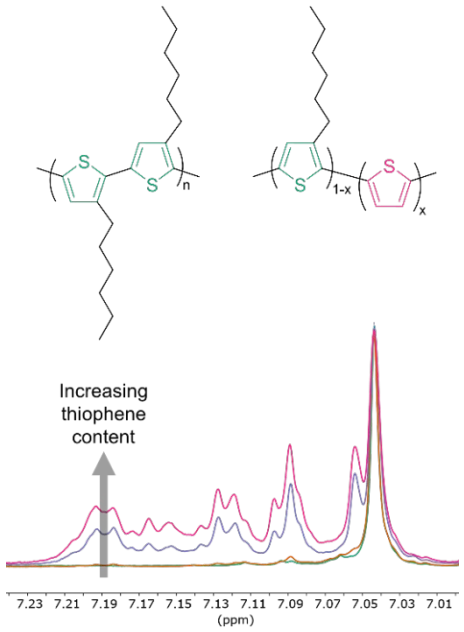

Figure 1. Representation of P3HT (left) and poly(3-hexylthiohene-*ran*-thiophene) (right). Green and pink thiophene units represent monomers with and without side chains respectively. x represents the mol% of unsubstituted thiophene. Superimposed ^{1}H NMR spectra of P3HT (green), T_{ref} (yellow), T19 (purple) and T24 (pink) focusing on the aromatic region (bottom).

Yamashita *et al.* reported the anion exchange doping method which allows for almost 100 % doping efficiency, substantially improving the electrical conductivity. [7]

Besides creating extra charge carriers, structural changes to the semiconductor film also occur upon doping.[8] Dopants can either co-crystalise with the semicrystalline polymer or disrupt the ordered packing, depending on the size and redox strength of the dopant, leading to a lower thermoelectric performance for the latter scenario. With this in mind, polymer-dopant pairs should be evaluated not only based on matching energetics for favourable electron transfer, but also based on steric considerations such as dopant size, polymer side chain density, and side chain interdigitation as well as non-covalent interactions between polymer and dopant.[9, 10]

Much work has been carried out recently on polythiophenes, trying to understand where dopants reside in the solid state and how they may affect the electrical conductivity. [11-15] Jacobs *et al.* recently showed that the overall crystalline structure of the film is the major driving force for high conductivity.[16] They conducted a study on a range of semiconducting polymers, including P3HT and PBTTT, and showed that increasing the anion size when using ion exchange doping, disrupted the packing to a greater extent, leading to lower conductivity. Doping of highly oriented semiconducting polymer films has also resulted in higher thermoelectric performance compared to non-aligned films. High temperature rubbing on semicrystalline polymer films leads to higher conductivity and Seebeck coefficients in the parallel direction to the rubbing direction due to aligned crystalline domains affording efficient charge transport.[17] However, high electrical conductivity in organic semiconductors usually require material design that produce highly crystalline films before doping or strategies to co-crystallise dopant and semiconductor.

Herein, we have used the benchmark polymer P3HT as a starting point for studying how side chain density can be used as a molecular design parameter for tuning polymer-dopant interactions and the thermoelectric performance of aligned and non-aligned doped polymer thin films. Similar to previous reports, we synthesised three random co-polymers comprising the two monomers thiophene and 3-hexylthiophene to afford Tx, where x represents the molar percentage of the unsubstituted thiophene co-monomer in the final polymer (Figure 1).[18] In other words, T24 means that, on average, for 76 thiophenes bearing a hexyl side chain there are 24 "naked" thiophenes without side chains. The positions of the units with and without side chains are randomly distributed in the polymer chain. The effect of randomly altering the side chain density in polythiophenes is well documented to improve the charge carrier mobility, however the effect on the thermoelectric properties is not so established.[19-26] For the non-aligned films, the electrical conductivity after doping with F4TCNQ increased gradually with decreasing side chain density, affording a 6-fold increase for the highest thiophene content (x = 24) compared to P3HT. On the other hand, polymer alignment by high-temperature rubbing proved less efficie [26] nt with decreasing side chain density. This is evidenced by decreasing dichroic ratios measured on the aligned films using polarised UV-Vis spectroscopy. As a consequence, electrical conductivity parallel to the direction of alignment was not clearly correlated to the side chain density due to the simultaneous decrease in melting temperature and lower degree of crystallinity with decreasing side chain density of the neutral polymer films.

RESULTS AND DISCUSSION

Characterisation of the Neutral Polymers. We synthesised the co-polymer series comprising thiophene and 3-hexylthiophene co-monomers using the Grignard metathesis (GRIM) method as previously reported (see SI Section 2 for details).[18, 27] The regioregularity (RR) of the P3HT reference batch synthesised was estimated to be 90% from high-temperature (90 °C) ^{1}H nuclear magnetic resonance (NMR) spectroscopy. We added 10, 20 and 30 mol% of 2,5-dibromothiophene to afford our random co-polymers with decreasing side chain density. From the ^{1}NMR NMR spectra, we estimated only 19 mol% and 24 mol% unsubstituted thiophene content as compared to feed ratios 20 mol% and 30 mol%, respectively and therefore named these polymers T19 and T24 (Figure 1 and Table 1). For the 10 mol% feed ratio, however, we calculated <<1 mol% (See SI for details) and the ^{1}H NMR spectrum closely

matches that of P3HT. Yet, increasing the intensity of the spectra reveals new peaks at 7.19 ppm not observed in the spectrum of P3HT. We therefore conclude that there is a very small amount of unsubstituted thiophene monomer in the polymer, however it is not significant enough to claim a number. The number-average molar mass measured using size exclusion chromatography (SEC) are comparable across the co-polymer series (~21-26 kg mol^{-1}) and show low dispersity (Đ) below 1.8 (Table 1). For P3HT, however, the number-average molecular weight is higher (40 kg mol^{-1}) and, as a note to the reader, the GPC trace of the P3HT batch used in this study exhibited a bimodal peak (Figure S7 and Table S2). For these reasons, we decided to use the batch with low thiophene content as a reference batch to better compare between similar molar masses across the polymer series, consequently naming the polymers P3HT, T_{ref}, T19 and T24.

Table 1. Comparison of the input/output thiophene contents, molar mass and thermal characteristics of all polymers.

Polymer	Output [Input] thiophene content (mol%)[a]	M_n (kg mol^{-1}) [Đ][b]	T_m/T_c (°C)[c]
P3HT	0	40 [1.3]	226/192
T_{ref}	<<1 [10]	23 [1.5]	221/191
T19	19 [20]	26 [1.8]	187/146
T24	24 [30]	21 [1.5]	146/110

[a]Output ratio estimated from ^{1}H NMR spectra recorded in d-TCE at 90 °C. [b]Number average molar mass (M_n) measured by size exclusion chromatography against polystyrene standards in chlorobenzene at 80°C. Đ = M_W/M_n. [c]Obtained by differential scanning calorimetry from the second heating and first cooling cycles recorded under nitrogen at 10 °C min^{-1}.

All polymers showed good thermal stability with thermal degradation occurring above 400 °C, determined using thermogravimetric analysis (Figure S8). At lower temperatures P3HT, T_{ref}, T19 and T24 showed endo- and exothermic events ascribed to the melting (T_m) and crystallisation (T_c) points respectively, observed from differential scanning calorimetry (DSC) measurements (Table 1 and Figure S8).[28] P3HT and T_{ref} exhibited a similar T_c around 190 °C and decreasing the side chain density leads to a decrease in T_c.[29] An exothermic event is also noted just below 100 °C for T_{ref} and T19 not exhibited by P3HT. The same peak might also appear in T24 however it is not clearly defined due to overlap with the T_c peak. The thermal results show that decreasing the side chain density leads to more non-crystalline films due to the decrease in intensity and temperature of the T_m/T_c peaks.

Solution UV-Vis absorbance spectroscopy of P3HT and T_{ref} in chlorobenzene revealed a S_0 to S_1 transition at very similar wavelengths around 455 nm, whereas T219 and T24 exhibited a red-shift of ~12 nm (Figure S9). Temperature dependent UV-Vis spectroscopy of the same solutions showed no change in the absorption maxima or shape of the bands when increasing the temperature from 20 to 100 °C suggesting no aggregation effects. We therefore attribute the red-shift observed for T19 and T24 to increased backbone planarity with higher thiophene content in agreement with previous density functional theory work on related systems.[18, 19, 30]

The energetics and microstructural changes in the solid state were investigated using UV-Vis absorbance spectroscopy on thin films spin-cast from ODCB. The spectra of P3HT and T_{ref} revealed one absorbance band arising from the S_0 to S_1 transition, exhibiting three shoulders at 606, 561 and 528 nm, ascribed to the 0-0, 0-1 and 0-2 vibronic transitions, respectively (Figure 2 and Table 2).[31, 32] The decreased side chain density in T19 and T24 resulted in a ~10 nm blue-shift of the thin film UV-Vis absorption maxima coinciding with a more intense 0-0 vibronic peak. The more intense 0-0 transition indicated increased planarity of the polymer backbone and intrachain coupling, agreeing with the solution UV-Vis spectra. We tentatively ascribe the un-expected blue-shift to a modified dielectric environment when less side chains are present. High temperature rubbing was used to further assess the effect of decreasing side chain density. Polymer films bar-coated onto sodium polystyrene sulfonate (NaPSS)-coated glass slides from 10 mg mL^{-1} ODCB solutions were mechanically rubbed using a microfibre cloth attached to a rotating cylinder while heating the substrate on a hot plate. Using polarized UV-Vis spectroscopy, the degree of alignment characterized by the

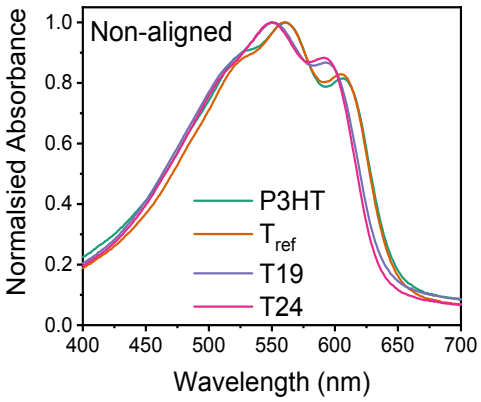

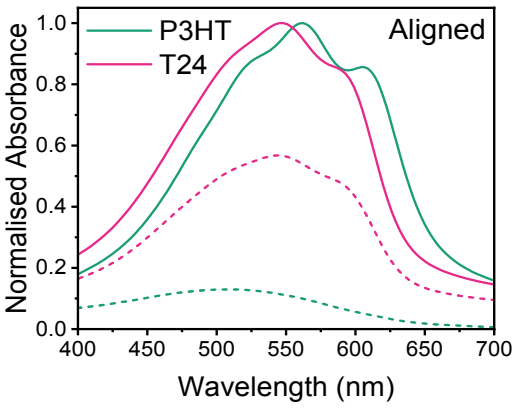

Figure 2. (top) UV-Vis absorbance spectra of P3HT, T_{ref}, T19 and T24 films spin-cast from 10 mg mL^{-1} o-dichlorobenzene (ODCB) solutions at 2000 rpm for 90 seconds. The spectra are normalised to the lambda max. (bottom) Polarised UV-Vis spectra of P3HT and T24 aligned films in the parallel (solid line) and perpendicular (dashed line) direction to the rubbing direction. P3HT and T24 films were rubbed at 220 °C and 80 °C respectively. The transitions in the parallel and perpendicular direction to the rubbing direction are normalised to the lambda max of the transition in the parallel direction.

Table 2. Optical and energetical properties of the neutral polymers.

Polymer	λ_{max} (nm)		E_g^{opt} (eV)[c]	DR [Rubbing Temperature] (°C)][d]	$E_{onset}^{(ox)}$ vs Fc/Fc^+ (V)[e]	Φ_{wf} (eV)[f]
	Solution[a]	Thin Film[b]				
P3HT	455	561	1.91	16 [220]	0.05	4.65
T_{ref}	456	560	1.91	10 [180]	0.06	4.67
T19	469	550	1.94	6 [150]	0.03	4.71
T24	471	549	1.95	3 [80]	0.03	4.70

[a]Measured by UV-Vis absorbance spectroscopy from 0.01 mg mL^{-1} polymer solutions in chlorobenzene set at 30 °C using a Peltier cooler. [b]Measured by UV-Vis absorbance spectroscopy from thin films spun from 10 mg mL^{-1} ODCB solutions at 80 °C at 2000 rpm for 90 seconds onto glass slides. [c]Estimated from the optical onset of absorbance. Energy (eV) = 1240 (eV nm) / λ (nm). [d]Dichroic ratio calculated using $DR = A_{\parallel}/A_{\perp}$. [e]Measured by cyclic voltammetry from the onset of oxidation of polymer thin films drop cast onto a glassy carbon electrode from 1 mg mL^{-1} chloroform solutions in acetonitrile with 0.1 M tetrabutylammonium hexafluorophosphate as the supporting electrolyte. A platinum wire, carbon electrode and Ag/Ag^+ electrode were used as the counter, working and reference electrodes respectively. $Fc/Fc^+ = Ag/Ag^+ - 0.115$ V. [f]Work function measured using PESA on two polymer thin films doctor bladed onto ITO coated glass from 10 mg mL^{-1} solutions in chlorobenzene.

dichroic ratio (DR) was estimated from the absorbance at 610 nm parallel and perpendicular to the rubbing directions. It has been extensively discussed in the literature that high temperature rubbing aligns the P3HT crystallites parallel to the rubbing direction, increasing the vibrationally structured absorption band associated to ordered polymer chains.[17, 33-35] On the other hand, the featureless, blue-shifted optical transition in the perpendicular direction to the rubbing direction arises from the absorption of non-aligned disordered polymer chains. We found that decreasing the side chain density lowered the in-plane alignment achieved by high temperature rubbing, clearly seen when comparing the maximum dichroic ratio at 610 nm from P3HT to T24 (Figure 2, Table 2 and Figure S11). Also, the similarity of the shape in the absorption peaks between the two directions showed that there are also ordered chains in the perpendicular direction to the rubbing direction. In addition, the temperature range over which optimal alignment occurs decreases substantially with lower side chain density. While T_{ref} behaves essentially as pure regioregular P3HT (as expected from the low unsubstituted thiophene content confirmed experimentally, Table 1) and can be rubbed at high temperature (180 °C), T24 displays a very different thermomechanical behaviour. According to the polarised UV-Vis spectra, the highest alignment of T24 occurs around 80 °C with a modest dichroic ratio of 3 compared to a dichroic ratio of 16 for P3HT rubbed at 220 °C. Alignment continuously drops for T24 films rubbed at higher temperatures and the film fully delaminates from the substrate at temperatures above 150 °C.

We studied the solid-state electrochemical properties across the polymer series using cyclic voltammetry (CV) and spectroelectrochemistry on non-aligned films (Figure 3, S12 and S14). P3HT and T_{ref} thin films drop-cast onto the carbon working electrode exhibited major electrochemical oxidation waves with peak currents at 0.5 V and 0.4 V vs Fc/Fc^+ respectively, along with minor oxidation waves with onsets at 0.05 V for both films when measuring at a scan rate of 50 mV s^{-1}.[11] Cyclic voltammograms of T19 and T24 revealed both these oxidative waves shifting to lower potentials, thereby indicating slightly smaller ionisation potentials by ~30 meV. We find this unexpected as removal of the side chains would increase the ionisation potential due to the loss from the inductive effect increasing the backbone electron density. We also measured the work function of thin films using photoelectron spectroscopy in air (PESA) and found a ~40 mV increase in energy upon incorporating >19 mol% thiophene content (Figure 3). Although the variations are small and possibly within the uncertainty of the measurements, the discrepancy between the CV and PESA techniques could arise due to measuring ion insertion into the film vs photoelectron emission respectively, where the former is largely dependent on morphology.[36] We also observed a decrease in ionisation potential between P3HT and T24 thin films spin-coated onto indium tin oxide (ITO) coated glass using spectroelectrochemistry (Figure 3). A steady decrease in absorbance of the λ_{max} for the neutral polymer vs potential was seen for P3HT thin films leading to an onset at +20 mV vs Fc/Fc^+, whereas a sharp decrease was observed for T24, resulting in an onset at -22 mV vs Fc/Fc^+. The sharper decrease of the neutral band with increasing potential observed for the novel polymer is of interest for electrochemical devices relying on the modulation of properties upon voltage application such as electrochromic devices and organic electrochemical transistors (OECTs).

To assess the effect of side chain density on the ordered structures within the solid state, we carried out diffraction on the aligned and non-aligned films. Grazing incidence x-

ray diffraction (GIXRD) carried out on non-aligned drop cast films of P3HT and T_{ref} in the out-of-plane direction showed similar diffraction patterns with the peak at 2θ = 5.5° characteristic of the (*h*00) lamellar stacking crystallites in edge-on orientation (Figure S19).[37] A stacking distance d_{100} was calculated to be 16.3 Å for P3HT and T_{ref} indicating similar crystal structure. On the other hand, diffraction patterns of T19 and T24 films showed much lower intensity of the (*h*00) peak resulting from lower structural order. A much smaller d_{100} of 15.2 and 14.6 Å was also observed for T19 and T24 films respectively. Appearance of a small peak at 2θ = 24.0° for T24 films, with an associated d-spacing of 3.7

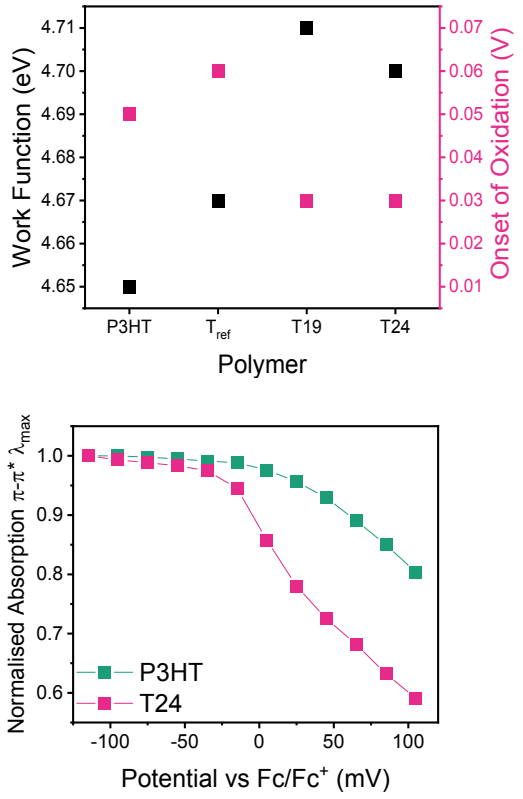

Figure 3. (top) Plot showing the correlations between work function and onset of electrochemical oxidation across the polymer series. The work function was obtained via the average of two PESA measurements on 10 mg mL^{-1} ODCB solutions doctor-bladed onto ITO substrates and the onset of oxidation was taken from the onset of the minor oxidation peak from the CV measurements at a scan rate of 50 mV s^{-1}. (bottom) Plot of the decrease in absorption of the π-π* transition of P3HT and T24 thin films spin-cast from 10 mg mL^{-1} ODCB solutions onto ITO-coated glass with increasing electrochemical potential. Each spectrum was taken 1 minute after the applied potential. The trend is normalised to the λ_{max} of the first spectrum taken in the undoped state.

Å that we assigned to (020) π-π stacking, also suggests a mix of edge-on and face-on orientation of the crystallites.

In rub-oriented films, decreasing the side chain density along the backbone again resulted in a lattice contraction in the (*h*00) direction, albeit smaller than observed for the non-aligned films. Most importantly, T24 rubbed thin films displayed no evidence for (*h*02) reflections from the electron diffraction patterns, further confirming a lack of long-range structural order in the stacking of T24 chains. In fact, the overall structure in T24 aligned films is alike the smectic-like phase observed for regioregular P3HT when rubbed at rubbing temperature of 100 °C.[33, 38]

We also observed a reduction in average surface roughness with decreasing side chain density of non-aligned films via atomic force microscopy (AFM) (Figure S20). P3HT and T_{ref} exhibit rough surfaces with an average roughness of 2.9 and 3.5 nm respectively, whereas T19 and T24 have smoother surface morphologies with an average roughness of 1.8 and 0.8 nm, respectively.

To summarize, decreasing the side chain density induces a lower degree of long-range order for both aligned and non-aligned films along with a contraction in the (*h*00) lattice parameter. Based on this evidence, we hence speculate that systematic removal of the side chains leads to the vacancies being filled by side chains on neighbouring monomers on the same polymer chain, therefore reducing the spacing between the backbones (Figure 4).

To investigate the effects of side chain vacancies on the charge transport properties, we fabricated bottom-gate, top-contact organic field effect transitions (OFETs) with non-aligned undoped polymer channels (refer to SI for details). All the polymers across the series showed p-type charge transport as expected. P3HT exhibits a saturation hole mobility of 1.1 x 10^{-4} cm^2 V^{-1} s^{-1} and the random co-polymers showed slightly higher values between 2 – 4 x 10^{-4} cm^2 V^{-1} s^{-1} tentatively ascribed to increased polymer chain connectivity through localised aggregates as discussed by Son *et al.* (Figure S26).[18] However, the charge carrier mobilities reported here did not reflect the large improvement observed in the previous literature upon removing ~30% alkyl side chains in polythiophenes and we believe that the observed differences in our study are not significant.

Thermoelectric Properties of the Doped Polymers. To explore the electrical properties of the doped polymer series, we doped non-aligned and aligned thin films with the widely studied oxidant F4TCNQ.[39] We doped the non-aligned films using the sequential processing (SqP) technique, using a combination of good and poor solvents which led to high and low doping levels, which we refer to as HighSqP and LowSqP, respectively (refer to SI for details).[35, 40-42] P3HT films doped with F4TCNQ under HighSqP and

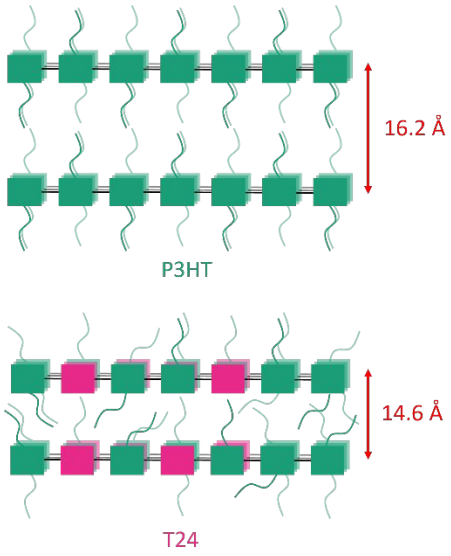

Figure 4. Schematic suggesting how the side chains fill empty space between the polymer backbones for T24 compared to P3HT, interpreted from the diffraction data of the non-aligned films. Green and pink squares represent thiophene monomers with and without a hexyl side chain respectively.

LowSqP conditions exhibited the lowest electrical conductivities in the series with a value around 3.1 and 0.3 S cm^{-1} respectively. With decreasing side chain density, we found that the conductivity increased gradually to a maximum value of 19.3 S cm^{-1} observed for HighSqP doped T24 films (Figure 5a). Interestingly T_{ref} films doped under both conditions showed over double the conductivity of P3HT, although T_{ref} displayed nearly identical structural order in the neutral films. To ensure the validity of our claims we also measured the conductivity of a P3HT batch with higher molecular weight and regioregularity doped with F4TCNQ under the same conditions (Table S7). We also found that T19 and T24 exhibited higher electrical conductivity under the same doping conditions as compared to this better performing batch of P3HT.

Turning our attention to the aligned films, we measured the conductivity parallel and perpendicular to the rubbing direction upon doping with 0.1 – 1 mg mL^{-1} F4TCNQ solutions in acetonitrile using the incremental concentration doping method (ICD) (Figure 5b).[35] In agreement with previous literature on highly orientated polymer films, the measured electrical conductivity of P3HT and the co-polymers films was much higher (~by one order of magnitude) in the parallel direction to rubbing as compared to the perpendicular direction (Figure S30). Alignment of the crystallites parallel to the rubbing direction improves charge carrier mobility in that direction. As a note here to the reader, we did not use the same doping conditions as above, as we were exploring the effects of high temperature rubbing not maximising performance. As established in the non-aligned films, the effect of decreasing side chain density improves the electrical conductivity, independent on doping conditions. At the highest F4TCNQ concentration (1 mg mL^{-1}) in the parallel direction, P3HT exhibited the highest conductivity of 193 S cm^{-1}, not T24, contrary to the trend observed with the non-aligned films. The observed trend with decreasing side chain density is fully consistent with the corresponding decrease in alignment of the polymer. The conductivity variation of the doped films as a function of side chain percentage reflects mainly the limited thermomechanical properties of the polythiophene with a low side chain density. We subsequently determined the Seebeck coefficients of the aligned doped films allowing us to estimate the Power Factor and hence evaluate the potential of the synthetic strategy proposed here for the design of semiconducting polymers for thermoelectric applications. At 1 mg mL^{-1} dopant concentration, the Seebeck coefficients in the parallel direction follow the same trend as the electrical conductivity, leading therefore to the Power Factor in the parallel direction also following the same trend (Figure 5b). Regardless of the structure of the polymer and the trend observed in non-aligned films, the conductivity and Seebeck coefficients parallel to the rubbing direction of the aligned

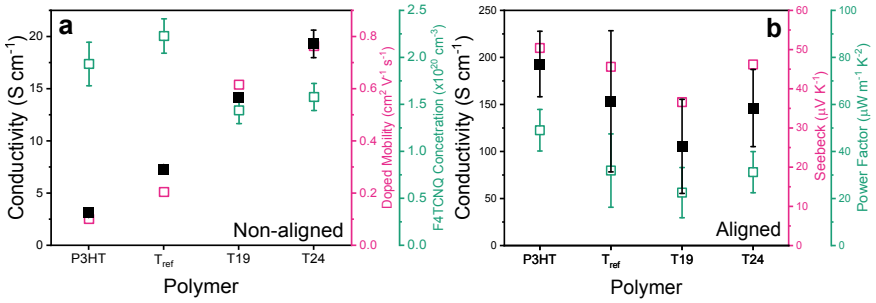

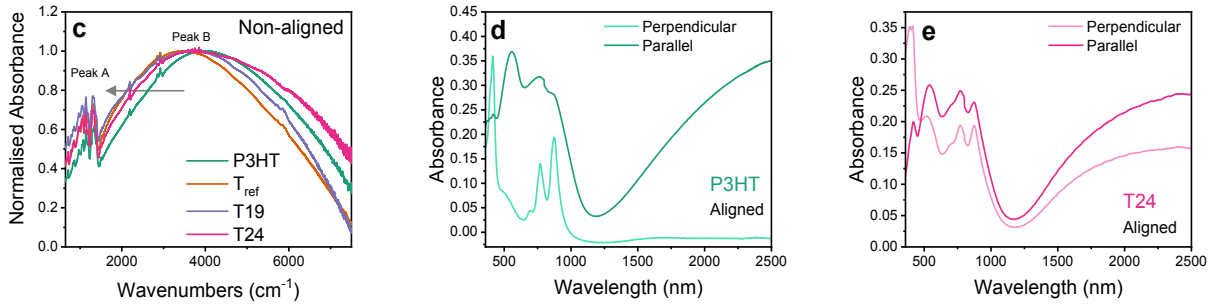

Figure 5. a) Plot showing the correlation between the measured electrical conductivity (black filled data points), estimated F4TCNQ radical anion concentration (pink filled) and estimated doped mobility (green open) for non-aligned P3HT and co-polymer thin films doped with F4TCNQ using HighSqP doping levels. The error bars arise from one standard deviation over 3 thickness measurements on one film and propagated through the Van der Pauw equation. b) Plot showing the correlation between the electrical conductivity (black filled), Seebeck Coefficient (pink open) and Power Factor (green open) in the parallel direction to the rubbing direction of aligned films doped with F4TCNQ at 1 mg mL^{-1}. The error bar in electrical conductivity arises from one standard deviation over two measurements of two devices. The error bar in Power Factor in propagated through PF = σS^2 where σ and S are the electrical conductivity and Seebeck coefficient respectively. See supplementary information section 14 for thickness calculations. c) FTIR spectra of P3HT and co-polymer doped non-aligned films. The arrow indicates to the reader the shift in the peak at ~4000 cm^{-1}. d,e) UV-Vis-NIR spectra of P3HT (d) and T24 (e) aligned films doped with F4TCNQ using ICD up to 1 mg mL^{-1} measured in the perpendicular and parallel directions to the rubbing direction.

films appeared to loosely follow the degree of alignment (quantified by the dichroic ratio, Table 2). We further explored the large improvement in conductivity observed in the non-aligned films and where the discrepancy between the aligned and non-aligned films arises from, as discussed below.

Characterisation of the Doped Films. UV-Vis absorbance spectroscopy carried out on the non-aligned doped films revealed a partial bleaching of the neutral band assigned to the polymer oxidation and four new peaks at 420, 697, 770 and 855 nm that are characteristics of F4TCNQ radical anion, confirming that integer charge transfer (ICT) has occurred (Figure S27 and S33 – 36).[43, 44] We fitted the absorbance spectra with Gaussians to estimate the F4TCNQ radical anion concentration and found that the density of ionised F4TCNQ is very similar for both HighSqP (~1.8 x 10^{20} ± 20 % cm^{-3}) and LowSqP (~1.0 x 10^{20} ± 12 % cm^{-3}) regardless of the thiophene content (Figure 4 and Table S8). This suggests that the significant improvement in conductivity of the non-aligned films did not arise from a larger charge carrier concentration in the doped films, but rather from an increase in the charge carrier mobility. Under the strong assumption that each F4TCNQ radical anion induces a mobile carrier, we estimated the charge carrier mobility within the doped films by dividing the measured conductivity by the calculated F4TCNQ radical anion density ($\sigma = \mu \cdot n$). We found that under HighSqP conditions, the estimated doped mobility increased significantly with decreasing side chain density. The maximum carrier mobility is hence found for doped T24 non-aligned films being four times larger than that of doped P3HT films (Figure 5a).

To confirm the improvement of carrier mobility with decreasing side chain density, we probed the changes in the P1 polaron peak across the polymer series using Fourier transform infra-red (FTIR) spectroscopy on doped non-aligned films (Figure 5c). From the normalised spectra, a red-shift of the large band at ~4000 cm^{-1} (Peak B) coinciding with increased intensity of the peak hidden by the so-called IR-active vibrations (IRAV) observed below 1500 cm^{-1} (Peak A) indicated stronger inter- and intrachain coupling in ordered polymers.[45, 46] Under HighSqP conditions, Peak B red-shifted further and Peak A increased in intensity for T_{ref}, T19 and T24 doped films when compared to P3HT doped films, pointing toward an even higher degree of polaron delocalisation. We note here that the broadening of Peak B suggests a larger distribution of localised and delocalised polarons compared to P3HT. These measurements suggest more uniform doping of both ordered and disordered. regions in T19 and T24, rationalizing the increased conductivity and mobility in these samples.[47]

To investigate the origin of the improved conductivity in the non-aligned films with decreasing side chain density, we measured the out-of-plane X-ray diffraction patterns of the drop cast non-aligned films doped by immersion in 2 mg mL^{-1} F4TCNQ solutions in acetonitrile overnight. The d_{100} lamellar distance for P3HT and T_{ref} films increased by ~2.5 Å from 16.3 Å in the neutral state to 18.8 – 18.9 Å in the doped state due to dopant insertion between the polymer backbones in the side chain region (Table S5).[48] T19 and T24 films also exhibited a lamellar expansion of ~2.7 Å upon dopant insertion and oxidation of the polymer backbone but retained a smaller d_{100} as compared to P3HT and T_{ref} (17.5 – 17.7 Å). Due to instrument capabilities, we only measured the out-of-plane direction, however we expect a parallel contraction in the π-stacking direction as previously reported.[27, 37] Concurrent with a smaller d_{100}, T19 and T24 doped films exhibited larger lamellar coherence lengths (~133 Å) compared to P3HT and T_{ref} doped films (~109 Å) demonstrating that doping the non-aligned films with lower side chain density induced longer range ordering. Comparing the X-ray diffraction patterns of the neutral and doped non-aligned films, the results suggest

that lowering the side chain density reduces the order in the neutral state compared to P3HT, however upon doping there are more ordered domains. This hypothesis agrees with the improved measured electrical conductivity and higher calculated charge carrier mobility of the doped films when lowering the side chain density.

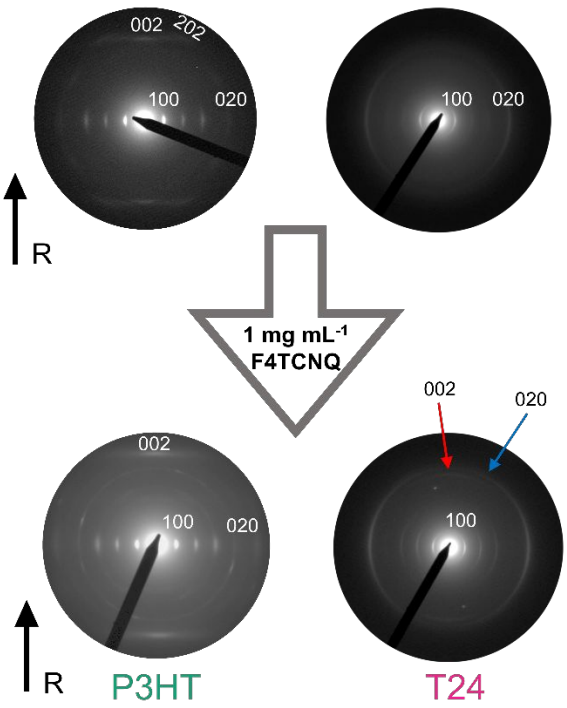

Figure 6. Electron diffraction patterns of P3HT and T24 aligned films before and after doping with F4TCNQ concentration of 1 mg mL^{-1}. The 'R' arrows represent the rubbing direction. The red and blue arrows direct the reader to the (002) and (020) reflection after doping to 1 mg mL^{-1} for T24 aligned films.

Turning our attention to the doped aligned films, we used polarised UV-Vis-NIR absorbance spectroscopy in the parallel and perpendicular direction to the rubbing direction. Aligned P3HT thin films displayed the F4TCNQ radical anion peaks in the perpendicular direction and the neutral and polaronic transitions in the parallel direction to the rubbing direction (Figure 5d). These findings agree with previous literature indicating that the F4TCNQ radical anions sit perpendicular to the oriented polymer backbone and that the films retain their anisotropy despite dopant insertion.[35] Doped aligned T_{ref} films showed almost identical spectra to P3HT suggesting a similarly high degree of alignment, again corroborating the strong similarity of P3HT and T_{ref} (Figure S34). However, all the optical transitions from both polymer and dopant are clearly observed in both the parallel and perpendicular directions for aligned and doped T19 and T24 films (Figure 5e and S35). The lack of anisotropy indicates a low degree of alignment of polymer backbones in the doped state. This likely arises from the relatively low dichroic ratio of undoped films as discussed above.

Electron diffraction using transmission electron microscopy (TEM) was used to probe the evolution of the microstructure as a function of increasing doping concentration on doped aligned films (Figure 6 and Figure S37). The impact of doping on the structure of T_{ref} films is almost identical to that observed for P3HT, further confirming the similarity between the two, where doping preserves the in-plane (edge-on) orientation of polymer chains. Electron diffraction showed the crystal lattice expanding in the side chain (lamellar) direction with an increase of d_{100} from 16.2 Å to 18.2 Å for P3HT and T_{ref} aligned films doped at 1 mg mL^{-1} F4TCNQ concentration, whereas the π-stacking periodicity (d_{020}) contracts from 3.7 Å to 3.6 Å. As observed previously for aligned regioregular P3HT, doping results in a notable change of intensity of the (*h*0l) lamellar stacking reflections (l = 0, 1, 2). The expansion of the (100) reflection and contraction of the (020) reflection also supports the results from the GIXRD measures of the non-aligned films, suggesting similar crystal structures between aligned and non-aligned films upon doping. The (002) end-to-end translational reflection becomes predominant with a total loss of intensity for (102) and (202) reflections, and as demonstrated in our previous work on F4TCNQ-doping of P3HT, this change in the electron diffraction pattern is a fingerprint of dopant intercalation into the crystal lattice of P3HT.[49]

For the two other polymers, T19 and T24, doping to 1 mg mL^{-1} F4TCNQ concentrations induced similar lattice modifications in the sense that the unit cell expanded in the side chain direction and contracted in the π-stacking direction. Compared to P3HT and T_{ref} however, the lattice parameter reached saturation at 0.1 mg mL^{-1} F4TCNQ concentration for T19 and T24 aligned films. Markedly, structural reorganisation in the aligned mesophase of T24 upon doping was observed more strongly than P3HT using electron diffraction, where the (002) reflection becomes visible after doping (Figure 6, red arrow). However, the appearance of this reflection for T24 doped films signifies a reorganisation of polymer chains within the π-stacks, such that the successive thiophene backbones shift in the chain axis direction to create some cavities to host the dopant molecules in the crystal lattice of the polymer. The same mechanism was observed for all polymers, regardless of the amount of unsubstituted thiophene in the backbone. However, it is possible that with increasing percentage of unsubstituted thiophene, the cost in reorganisation of the backbones within π-stacks was reduced and therefore the effect is observed more strongly with decreasing side chain density.

CONCLUSIONS

Using the benchmark semiconducting polymer P3HT as our model system, we studied systematically how the side chain density influences optical and electronic properties of non-aligned and aligned films in views of thermoelectric applications. A simple synthetic protocol provides low-cost

access to thiophene and 3-hexylthiophene random copolymers with varying content of unsubstituted thiophenes (and thus side chain vacancies) by controlling the monomer feed ratios. Despite a 10 mol% feed ratio, polymer T_{ref} actually showed <1 mol% of side chain vacancies making it structurally very similar to P3HT, thus resulting in very similar optical and electronic properties to P3HT. Increasing the unsubstituted thiophene content to 20% and 30% afforded polymers T19 and T24 with better agreement between feed ratios and observed degrees of side chain vacancies. For the non-aligned polymer films, the electrical conductivity after doping with F4TCNQ increased markedly with decreasing side chain density; a more than 6-fold increase from 3.1 to 19.3 S cm^{-1} was observed for T24 compared to P3HT under high doping conditions. While the F4TCNQ radical anion concentration remains fairly constant across the copolymer series upon doping, a significant increase in the estimated doped charge carrier mobility is observed for the copolymers with lower side chain densities. A recent study by Kim *et al.* has also observed the same trend upon doping a similar co-polymer system with F4TCNQ. Albeit at lower electrical conductivity, they observed an increase in electrical conductivity of thin films with more thiophene co-monomer when doping via blending in solution.[25]

As a simple synthetic tool, we thus find that introducing side chain vacancies does not – perhaps somewhat contrary to simplistic consideration regarding the extra free volume – allow for higher charge carrier concentrations during doping. On the other hand, the introduction of side chain vacancies makes the T19 and T24 copolymers more facile to structural reorganisation upon doping. This is evidenced by our electron diffraction studies where the (002) reflection of T24 becomes visible after doping and by x-ray diffraction studies where longer crystallite coherence lengths are measured for the doped T24 films when compared to doped P3HT films. These findings are corroborated by the higher charge carrier mobilities extracted for the doped films with lower side chain densities, which ultimately lead to the observed trend of increasing electrical conductivity with decreasing side chain density.

However, thermal rubbing proved less efficient with decreasing side chain density, evident from decreasing dichroic ratios measured on the aligned films using polarised UV-Vis absorbance spectroscopy. Therefore, electrical conductivity parallel to the direction of alignment was not clearly correlated to the degree of side chain vacancies due to the simultaneous change in melting temperature of the polymers. Although decreasing the side chain density allowed for beneficial reorganisation of the non-aligned films upon doping, these attributes prevent a high degree of structural alignment by thermal rubbing. That being said, T24 aligned doped films showed a comparable Power Factor (31 μW $m^{-1} K^{-2}$) to P3HT (49 μW $m^{-1} K^{-2}$) even with a very low dichroic ratio.

Our results therefore suggest that side chain engineering – and in particular introducing unsubstituted monomer units - can be an effective way to fine-tune the degree of order/disorder of the conjugated polymer to suit the intended application. This simple synthetic method could lead to low-cost materials suited to cheap large scale device fabrication techniques *i.e.,* roll-to-roll printing. Although our initial attempts at alignment prior to doping do not lead to enhanced electrical conductivity, we anticipate that further optimisation of dichroic ratio with low side chain density could afford further improvements.

EXPERIMENTAL SECTION

Materials. 3-hexylthiophene and dichloro(1,3-bis(diphenylphosphino)propane)nickel ($Ni(dppp)Cl_2$) were purchased from Fluorochem. N-bromosuccinimide (NBS) and isopropyl magnesium chloride lithium chloride solution (1.3 M in THF) were purchased from Sigma-Aldrich. 2,5-dibromothiophene was purchased from Tokyo Chemical Industry. 2,3,5,6-Tetrafluoro-7,7,8,8-tetracyanoquinodimethane (F4TCNQ) was purchased from Ossila or Sigma-Aldrich. $CDCl_3$ and deuterated tetrachloroethane (d_2-TCE) was purchased from Cambridge isotopes. Dry tetrahydrofuran (THF) (99.5% over molecular sieves with AgroSeal) and dry dimethylformamide (DMF) (99.5% over molecular sieves with AgroSeal) were purchased from Acros Organics. Ortho-dichlorobenzene (ODCB) was purchased from either Acros Organics or Sigma-Aldrich. Unless stated all other solvents are HPLC grade purchased from Honeywell. All chemicals were used as purchased without further purification. Details of the synthesis of P3HT, T_{ref}, T19 and T24 and NMR characterisation is described in the supporting information.

General Experimental Details. GPC was performed on the Shimadzu Prominence GPC system using chlorobenzene as the mobile phase at flow rate of 1 mL min^{-1}. The molar mass of each polymer was measured against polystyrene standards. TGA was carried out on TA instruments Q500 under N_2 at 10 °C min^{-1}. DSC was performed using a TA Instruments DSC25 under N_2 at 10 °C min^{-1} Unless mentioned thin films were fabricated from spin coated 10 mg mL^{-1} ODCB solutions at 2000 rpm for 90 s then 8000 rpm for 30 s. UV-Vis spectroscopy of the non-aligned and aligned films was carried out on a Shimadzu UV3600 UV-Vis-NIR spectrometer and Varian Cary5000 spectrometer. FTIR spectroscopy was carried out on a Bruker Vertex 70v FT-IR spectrometer under vacuum using a DLaTGS detector. CV experiments were conducted using a Palm EmStat3 with the reference, counter and working electrodes as Ag/Ag^+, platinum and glassy carbon. 1 mg ml^{-1} chloroform solutions of each polymer were dropcast onto the working electrode. 0.1 M tetrabutylammonium hexafluorophosphate in N_2 degassed acetonitrile was used as the supporting electrolyte. Spectroelectrochemical experiments was carried out using the same set up but thin films of P3HT and T24 were spin coated onto ITO substrates as the working electrode and the UV-Vis spectra were measured using a Shimadzu UV3600 UV-Vis-NIR spectrometer. PESA was performed on polymer thin films, doctor bladed from 10 mg mL^{-1} ODCB solutions onto ITO coated glass and measured using an AC-2 Model from Riken Instruments. GIXRD was carried out on dropcast films from 20 mg mL^{-1} ODCB polymer solutions onto silicon substrates and measured using a PANalytical X'Pert Pro diffractometer. AFM was carried out on polymer thin films using a Bruker Dimension Icon System. ScanAsyst Air tips were used to image the samples in PeakForce Quantitative Nanomechanical Property Mapping (QNM) mode. TEM ED

patterns were obtained using a CM12 Philips microscope equipped with a MVII (Soft Imaging System) camera on polymers films coated with a thin amorphous carbon film and floated onto a TEM copper grid.

OFET Device Fabrication. The back-gate and gate dielectrics were chosen to be highly n-doped silicon and thermally grown SiO_2 (300 nm), respectively. After cleaning Si/SiO_2 substrates with oxygen plasma at 300W for 10 min, the substrates were then immersed in 3 wt% PTS/toluene solution for 15 hours at 90 °C. The excess PTS on Si/SiO_2 substrates were cleaned by sonication with toluene, followed by toluene, acetone and isopropanol rinse. The polymers solutions were pre-heated at 80°C for 1-2 hours before film deposition. The polymers (10 mg mL^{-1}) in ODCB were spin-coated on PTS-functionalized Si wafer. The Cr/Au electrodes (5/250 nm) were thermally evaporated under high vacuum (10^{-6} mbar) as the source and drain electrodes (W/L = 1000/20). The prepared OFETs were placed in a nitrogen glove box prior to testing.

Polymer thin film alignment. The aligned polymer films were prepared by doctor-blading a hot solution in ODCB (10 mg mL^{-1}) at 160 °C on cleaned glass slides covered with a sacrificial polymer film of water-soluble NaPSS (10 mg mL^{-1} aq). The orientation of the films by high-temperature rubbing followed the protocol described in previous publications.[33, 50] Rubbing is performed by using a homemade set-up. It consists of a rotating cylinder covered with a polyester cloth and a translating hot plate.

Thermoelectric Characterisation Details. The electrical conductivity of the F4TCNQ doped non-aligned polymer thin films was measured on a Karl Suss probe station under a nitrogen atmosphere using an Agilent 4155B source meter following the standard Van der Pauw method. The non-aligned films were doped using sequential doping methods as the oxidant as described in the supporting information. The electrical conductivity of the F4TCNQ doped aligned films was measured using a Keithley 2634B source meter and a Lab Assistant Semiprobe station under a nitrogen atmosphere. Aligned thin films were transferred to substrates with gold contacts with a linear four-point probe geometry. The Seebeck coefficient was measured using a differential temperature method on the same devices, by varying the temperature gradient across the substrate and measuring the corresponding thermovoltage.

ASSOCIATED CONTENT

The supporting information is free of charge on the ASC Publications website at DOI:

Synthetic procedures for the monomers and polymers, nuclear magnetic resonance spectra, gel permeation chromatography data, thermal characterization analysis, thin film and solution UV-Vis-NIR spectroscopy of the aligned and non-aligned films in the doped and neutral state, electrochemical and spectroelectrochemical experiments, work function measurements, roughness measurements, transistor fabrication and analysis, conductivity measurements of the aligned and non-aligned films, fittings of the UV-Vis spectra of the doped non-aligned thin films, Fourier transform infra-red spectra of the non-aligned doped films, X-ray diffraction analysis of the drop cast thick films, method for producing highly orientated thin films, data extracted from the electron diffraction patterns, calibration curves used to estimate the thickness of the aligned thin films.

AUTHOR INFORMATION

Corresponding Authors

*Email (P.A.GF): p.finn@ucl.ac.uk
*Email (C.B.N): c.b.nielsen@qmul.ac.uk

Orcid

Peter A. Gilhooly-Finn: 0000-0002-5113-8873
Ian E. Jacobs: 0000-0002-1535-4608
Olivier Bardagot: 0000-0003-3306-7204
Matteo Palma: 0000-0001-8715-4034
Natalie Banerji: 0000-0001-9181-2642
Henning Sirringhaus: 0000-0001-9827-6061
Martin Brinkmann: 0000-0002-2680-1506
Christian B. Nielsen: 0000-0002-8591-1203

Notes

The authors declare no competing financial interest.

ACKNOWLEDGMENT

We acknowledge the European Commission for financial support through the MITICS H2020-EU-FET Open project (No. 964677). P.A.GF would like to acknowledge Richard Whiteley for running the X-ray diffraction experiments. M.B. acknowledges financial support from ANR contract ANR-17-CE05-0012. H.S. acknowledges funding from the European Research Council (ERC, Grant 101020872) and the Royal Society (RP\R1\201082). O.B. and N.B. thank the European Commission for financial support through the OSIRIS ERC Starting Grant (No. 714586), as well as the University of Bern.

REFERENCES

(1) Finn, P. A.; Asker, C.; Wan, K.; Bilotti, E.; Fenwick, O.; Nielsen, C. B. Thermoelectric Materials: Current Status and Future Challenges. *Frontiers in Electronic Materials* **2021**, *1*.

(2) Zhao, Y.; Liu, L. Y.; Zhang, F. J.; Di, C. A.; Zhu, D. B. Advances in organic thermoelectric materials and devices for smart applications. *Smartmat* **2021**, *2* (4), 426-445.

(3) Wang, S. H.; Peng, L.; Sun, H. B.; Huang, W. The future of solution processing toward organic semiconductor devices: a substrate and integration perspective. *Journal of Materials Chemistry C* **2022**, *10* (35), 12468-12486.

(4) Bronstein, H.; Nielsen, C. B.; Schroeder, B. C.; McCulloch, I. The role of chemical design in the performance of organic semiconductors. *Nature Reviews Chemistry* **2020**, *4* (2), 66-77.

(5) Zhang, F. J.; Di, C. A. Exploring Thermoelectric Materials from High Mobility Organic Semiconductors. *Chemistry of Materials* **2020**, *32* (7), 2688-2702.

(6) Bardagot, O.; Aumaître, C.; Monmagnon, A.; Pécaut, J.; Bayle, P.-A.; Demadrille, R. Revisiting doping mechanisms of n-type organic materials with N-DMBI for thermoelectric applications: Photo-activation, thermal activation, and air stability. *Applied Physics Letters* **2021**, *118* (20).

(7) Yamashita, Y.; Tsurumi, J.; Ohno, M.; Fujimoto, R.; Kumagai, S.; Kurosawa, T.; Okamoto, T.; Takeya, J.; Watanabe, S. Efficient molecular doping of polymeric semiconductors driven by anion exchange. *Nature* **2019**, *572* (7771), 634-638.

(8) Nightingale, J.; Wade, J.; Moia, D.; Nelson, J.; Kim, J. S. Impact of Molecular Order on Polaron Formation in Conjugated Polymers. *Journal of Physical Chemistry C* **2018**, *122* (51), 29129-29140.

(9) Karpov, Y.; Erdmann, T.; Raguzin, I.; Al-Hussein, M.; Binner, M.; Lappan, U.; Stamm, M.; Gerasimov, K. L.; Beryozkina, T.; Bakulev, V.; et al. High Conductivity in Molecularly p-Doped Diketopyrrolopyrrole-Based Polymer: The Impact of a High

Dopant Strength and Good Structural Order. *Adv Mater* **2016**, *28* (28), 6003-6010.

(10) Liu, J.; Qiu, L.; Alessandri, R.; Qiu, X.; Portale, G.; Dong, J.; Talsma, W.; Ye, G.; Sengrian, A. A.; Souza, P. C. T.; et al. Enhancing Molecular n-Type Doping of Donor-Acceptor Copolymers by Tailoring Side Chains. *Adv Mater* **2018**, *30* (7).

(11) Cavassin, P.; Holzer, I.; Tsokkou, D.; Bardagot, O.; Rehault, J.; Banerji, N. Electrochemical Doping in Ordered and Disordered Domains of Organic Mixed Ionic-Electronic Conductors. *Adv Mater* **2023**, e2300308.

(12) Lim, E.; Peterson, K. A.; Su, G. M.; Chabinyc, M. L. Thermoelectric Properties of Poly(3-hexylthiophene) (P3HT) Doped with 2,3,5,6-Tetrafluoro-7,7,8,8-tetracyanoquinodimethane (F4TCNQ) by Vapor-Phase Infiltration. *Chemistry of Materials* **2018**, *30* (3), 998-1010.

(13) Neusser, D.; Malacrida, C.; Kern, M.; Gross, Y. M.; van Slageren, J.; Ludwigs, S. High Conductivities of Disordered P3HT Films by an Electrochemical Doping Strategy. *Chemistry of Materials* **2020**, *32* (14), 6003-6013.

(14) Dong, B. X.; Nowak, C.; Onorato, J. W.; Ma, T. Z.; Niklas, J.; Poluektov, O. G.; Grocke, G.; DiTusa, M. F.; Escobedo, F. A.; Luscombe, C. K.; et al. Complex Relationship between Side-Chain Polarity, Conductivity, and Thermal Stability in Molecularly Doped Conjugated Polymers. *Chemistry of Materials* **2021**, *33* (2), 741-753.

(15) Watts, K. E.; Neelamraju, B.; Ratcliff, E. L.; Pemberton, J. E. Stability of Charge Transfer States in F4TCNQ-Doped P3HT. *Chemistry of Materials* **2019**, *31* (17), 6986-6994.

(16) Jacobs, I. E.; D'Avino, G.; Lemaur, V.; Lin, Y.; Huang, Y.; Chen, C.; Harrelson, T. F.; Wood, W.; Spalek, L. J.; Mustafa, T.; et al. Structural and Dynamic Disorder, Not Ionic Trapping, Controls Charge Transport in Highly Doped Conducting Polymers. *J Am Chem Soc* **2022**, *144* (7), 3005-3019.

(17) Hamidi-Sakr, A.; Biniek, L.; Bantignies, J. L.; Maurin, D.; Herrmann, L.; Leclerc, N.; Leveque, P.; Vijayakumar, V.; Zimmermann, N.; Brinkmann, M. A Versatile Method to Fabricate Highly In-Plane Aligned Conducting Polymer Films with Anisotropic Charge Transport and Thermoelectric Properties: The Key Role of Alkyl Side Chain Layers on the Doping Mechanism. *Advanced Functional Materials* **2017**, *27* (25).

(18) Son, S. Y.; Kim, Y.; Lee, J.; Lee, G. Y.; Park, W. T.; Noh, Y. Y.; Park, C. E.; Park, T. High-Field-Effect Mobility of Low-Crystallinity Conjugated Polymers with Localized Aggregates. *J Am Chem Soc* **2016**, *138* (26), 8096-8103.

(19) Park, K. H.; Son, S. Y.; Kim, J. O.; Kang, G.; Park, T.; Kim, D. Role of Disorder in the Extent of Interchain Delocalization and Polaron Generation in Polythiophene Crystalline Domains. *J Phys Chem Lett* **2018**, *9* (12), 3173-3180.

(20) Son, S. Y.; Choi, K.; Lee, J.; Kim, H. I.; Park, T.; Kim, M. Backbone Randomization in Conjugated Polymer-Based Hole-Transport Materials to Enhance the Efficiencies of Perovskite Solar Cells. *Chemistry of Materials* **2022**, *34* (11), 4856-4864.

(21) Janus, K.; Chlebosz, D.; Janke, A.; Goldeman, W.; Kiersnowski, A. Contributions of Polymer Chain Length, Aggregation and Crystallinity Degrees in a Model of Charge Carrier Transport in Ultrathin Polymer Films. *Macromolecules* **2023**, *56* (3), 964-973.

(22) Chen, Z.; Huang, J.; Gao, D.; Yang, J.; Zhang, W.; Ju, H.; Yu, G. Highly-soluble multi-alkylated polymer semiconductors and applications in high-performance field-effect transistors. *Journal of Materials Chemistry C* **2019**, *7* (31), 9591-9598.

(23) Chai, H.; Xu, Z.; Li, H.; Zhong, F.; Bai, S.; Chen, L. Sequential-Twice-Doping Approach toward Synergistic Optimization of Carrier Concentration and Mobility in Thiophene-Based Polymers. *ACS Applied Electronic Materials* **2022**, *4* (10), 4947-4954.

(24) Son, S. Y.; Park, T.; You, W. Understanding of Face-On Crystallites Transitioning to Edge-On Crystallites in Thiophene-Based Conjugated Polymers. *Chemistry of Materials* **2021**, *33* (12), 4541-4550.

(25) Kim, J.; Guo, J.; Sini, G.; Sørensen, M. K.; Andreasen, J. W.; Woon, K. L.; Coropceanu, V.; Paleti, S. H. K.; Wei, H.; Peralta, S.; et al. Remarkable conductivity enhancement in P-doped polythiophenes via rational engineering of polymer-dopant interactions. *Materials Today Advances* **2023**, *18*.

(26) Stewart, K.; Pagano, K.; Tan, E.; Daboczi, M.; Rimmele, M.; Luke, J.; Eslava, S.; Kim, J. S. Understanding Effects of Alkyl Side-Chain Density on Polaron Formation Via Electrochemical Doping in Thiophene Polymers. *Adv Mater* **2023**, e2211184.

(27) Finn, P. A.; Jacobs, I. E.; Armitage, J.; Wu, R. H.; Paulsen, B. D.; Freeley, M.; Palma, M.; Rivnay, J.; Sirringhaus, H.; Nielsen, C. B. Effect of polar side chains on neutral and p-doped polythiophene. *Journal of Materials Chemistry C* **2020**, *8* (45), 16216-16223.

(28) Yu, L.; Davidson, E.; Sharma, A.; Andersson, M. R.; Segalman, R.; Muller, C. Isothermal Crystallization Kinetics and Time-Temperature-Transformation of the Conjugated Polymer: Poly(3-(2'-ethyl)hexylthiophene). *Chem Mater* **2017**, *29* (13), 5654-5662.

(29) Fei, Z.; Boufflet, P.; Wood, S.; Wade, J.; Moriarty, J.; Gann, E.; Ratcliff, E. L.; McNeill, C. R.; Sirringhaus, H.; Kim, J. S.; et al. Influence of Backbone Fluorination in Regioregular Poly(3-alkyl-4-fluoro)thiophenes. *J Am Chem Soc* **2015**, *137* (21), 6866-6879.

(30) Son, S. Y.; Kim, J.-H.; Song, E.; Choi, K.; Lee, J.; Cho, K.; Kim, T.-S.; Park, T. Exploiting π–π Stacking for Stretchable Semiconducting Polymers. *Macromolecules* **2018**, *51* (7), 2572-2579.

(31) Spano, F. C.; Silva, C. H- and J-aggregate behavior in polymeric semiconductors. *Annu Rev Phys Chem* **2014**, *65*, 477-500.

(32) Hestand, N. J.; Spano, F. C. Expanded Theory of H- and J-Molecular Aggregates: The Effects of Vibronic Coupling and Intermolecular Charge Transfer. *Chem Rev* **2018**, *118* (15), 7069-7163.

(33) Hamidi-Sakr, A.; Biniek, L.; Fall, S.; Brinkmann, M. Precise Control of Lamellar Thickness in Highly Oriented Regioregular Poly(3-Hexylthiophene) Thin Films Prepared by High-Temperature Rubbing: Correlations with Optical Properties and Charge Transport. *Advanced Functional Materials* **2016**, *26* (3), 408-420.

(34) Untilova, V.; Hynynen, J.; Hofmann, A. I.; Scheunemann, D.; Zhang, Y.; Barlow, S.; Kemerink, M.; Marder, S. R.; Biniek, L.; Muller, C.; et al. High Thermoelectric Power Factor of Poly(3-hexylthiophene) through In-Plane Alignment and Doping with a Molybdenum Dithiolene Complex. *Macromolecules* **2020**, *53* (15), 6314-6321.

(35) Vijayakumar, V.; Durand, P.; Zeng, H.; Untilova, V.; Herrmann, L.; Algayer, P.; Leclerc, N.; Brinkmann, M. Influence of dopant size and doping method on the structure and thermoelectric properties of PBTTT films doped with F6TCNNQ and F4TCNQ. *Journal of Materials Chemistry C* **2020**, *8* (46), 16470-16482.

(36) DiTullio, B. T.; Savagian, L. R.; Bardagot, O.; De Keersmaecker, M.; Osterholm, A. M.; Banerji, N.; Reynolds, J. R. Effects of Side-Chain Length and Functionality on Polar Poly(dioxythiophene)s for Saline-Based Organic Electrochemical Transistors. *J Am Chem Soc* **2023**, *145* (1), 122-134.

(37) Nagamatsu, S.; Pandey, S. S. Ordered arrangement of F4TCNQ anions in three-dimensionally oriented P3HT thin films. *Sci Rep* **2020**, *10* (1), 20020.

(38) Untilova, V.; Biskup, T.; Biniek, L.; Vijayakumar, V.; Brinkmann, M. Control of Chain Alignment and Crystallization Helps Enhance Charge Conductivities and Thermoelectric Power Factors in Sequentially Doped P3HT:F4TCNQ Films. *Macromolecules* **2020**, *53* (7), 2441-2453.

(39) Hynynen, J.; Kiefer, D.; Yu, L.; Kroon, R.; Munir, R.; Amassian, A.; Kemerink, M.; Muller, C. Enhanced Electrical Conductivity of

Molecularly p-Doped Poly(3-hexylthiophene) through Understanding the Correlation with Solid-State Order. *Macromolecules* **2017**, *50* (20), 8140-8148.

(40) Jacobs, I. E.; Aasen, E. W.; Oliveira, J. L.; Fonseca, T. N.; Roehling, J. D.; Li, J.; Zhang, G. W.; Augustine, M. P.; Mascal, M.; Moule, A. J. Comparison of solution-mixed and sequentially processed P3HT:F4TCNQ films: effect of doping-induced aggregation on film morphology. *Journal of Materials Chemistry C* **2016**, *4* (16), 3454-3466.

(41) Chew, A. R.; Ghosh, R.; Shang, Z.; Spano, F. C.; Salleo, A. Sequential Doping Reveals the Importance of Amorphous Chain Rigidity in Charge Transport of Semi-Crystalline Polymers. *J Phys Chem Lett* **2017**, *8* (20), 4974-4980.

(42) Fontana, M. T.; Stanfield, D. A.; Scholes, D. T.; Winchell, K. J.; Tolbert, S. H.; Schwartz, B. J. Evaporation vs Solution Sequential Doping of Conjugated Polymers: F4TCNQ Doping of Micrometer-Thick P3HT Films for Thermoelectrics. *The Journal of Physical Chemistry C* **2019**, *123* (37), 22711-22724.

(43) Watts, K. E.; Clary, K. E.; Lichtenberger, D. L.; Pemberton, J. E. FTIR Spectroelectrochemistry of F4TCNQ Reduction Products and Their Protonated Forms. *Anal Chem* **2020**, *92* (10), 7154-7161.

(44) Mendez, H.; Heimel, G.; Winkler, S.; Frisch, J.; Opitz, A.; Sauer, K.; Wegner, B.; Oehzelt, M.; Rothel, C.; Duhm, S.; et al. Charge-transfer crystallites as molecular electrical dopants. *Nat Commun* **2015**, *6*, 8560.

(45) Scholes, D. T.; Yee, P. Y.; Lindemuth, J. R.; Kang, H.; Onorato, J.; Ghosh, R.; Luscombe, C. K.; Spano, F. C.; Tolbert, S. H.; Schwartz, B. J. The Effects of Crystallinity on Charge Transport and the Structure of Sequentially Processed F(4)TCNQ-Doped Conjugated Polymer Films. *Advanced Functional Materials* **2017**, *27* (44).

(46) Ghosh, R.; Pochas, C. M.; Spano, F. C. Polaron Delocalization in Conjugated Polymer Films. *Journal of Physical Chemistry C* **2016**, *120* (21), 11394-11406.

(47) Chen, C.; Jacobs, I. E.; Kang, K.; Lin, Y.; Jellett, C.; Kang, B.; Lee, S. B.; Huang, Y.; BaloochQarai, M.; Ghosh, R.; et al. Observation of Weak Counterion Size Dependence of Thermoelectric Transport in Ion Exchange Doped Conducting Polymers Across a Wide Range of Conductivities. *Advanced Energy Materials* **2023**, *13* (9).

(48) Thomas, E. M.; Brady, M. A.; Nakayama, H.; Popere, B. C.; Segalman, R. A.; Chabinyc, M. L. X-Ray Scattering Reveals Ion-Induced Microstructural Changes During Electrochemical Gating of Poly(3-Hexylthiophene). *Advanced Functional Materials* **2018**, *28* (44).

(49) Untilova, V.; Zeng, H.; Durand, P.; Herrmann, L.; Leclerc, N.; Brinkmann, M. Intercalation and Ordering of F6TCNNQ and F4TCNQ Dopants in Regioregular Poly(3-hexylthiophene) Crystals: Impact on Anisotropic Thermoelectric Properties of Oriented Thin Films. *Macromolecules* **2021**, *54* (13), 6073-6084.

(50) Biniek, L.; Pouget, S.; Djurado, D.; Gonthier, E.; Tremel, K.; Kayunkid, N.; Zaborova, E.; Crespo-Monteiro, N.; Boyron, O.; Leclerc, N.; et al. High-Temperature Rubbing: A Versatile Method to Align π-Conjugated Polymers without Alignment Substrate. *Macromolecules* **2014**, *47* (12), 3871-3879.

Table of Contents Image